Cathode thermal effects in one-dimensional space-charge-limited electron flow

Stanley Humphries, Ph.D.

Field Precision LLC
E mail: techinfo@fieldp.com
Internet: https://www.fieldp.com

1 Introduction

The space-charge-limited flow of electrons across a vacuum acceleration gap is a process of practical importance in the design of wide variety of electron-beam equipment. The theory of flow with a singular electron distribution (zero kinetic energy at the cathode) is familiar and easily understood. It was developed in 1911 by C.D. Child[1]. The theory becomes much more difficult when electrons are emitted from a high-temperature cathode with an initial kinetic-energy distribution[2, 3, 4]. The analytic theory of Langmuir[5] describes the physics of thermal sheath formation and electron selection. Although the theory is important in the history of science, it involves so many equations, variables and limiting conditions that it is doubtful that it is generally applied. Nonetheless, thermal effects are important in the design of electron injectors and modeling codes:

> For low-voltage injectors, initial electron thermal energy increases the space-charge-limited current density.
>
> Transverse components of thermal energy limit the emittance of the extracted beam.

This paper describes numerical solutions for the space-charge-limited flow of hot electrons. With a numerical method, approximations that limit the range of validity are not necessary. My primary goal was to create a set of equations and graphs that could be applied easily by design engineers. The results apply to both non-relativistic electron and ion extractors. In addition, I wanted to determine whether selection processes at a thermal sheath could influence the transverse temperature of extracted electrons.

Consider an acceleration gap of width d in the z direction with infinite extent in x and y. The cathode at position $z = 0.0$ has potential $\phi = 0.0$ V. The anode at $z = d$ has $\phi = -V_0$. Suppose there is an unlimited source of electrons with zero kinetic energy at the cathode surface. Some of these electrons are extracted from the cathode by the applied electric field. The negative space-charge of the transported electrons lowers the average potential in the gap, reducing the magnitude of the electric field at the cathode. At a limiting value of current density, the surface field is reduced to zero (Fig. 1a) A higher value of current density would create a decelerating surface field, inconsistent with the extraction of the zero-energy electrons. The Child limit[1] is given by

$$j_c = \left(\frac{4\epsilon_o}{9}\right) \sqrt{\frac{2e}{m_e}} \frac{V_o^{3/2}}{d^2}. \tag{1}$$

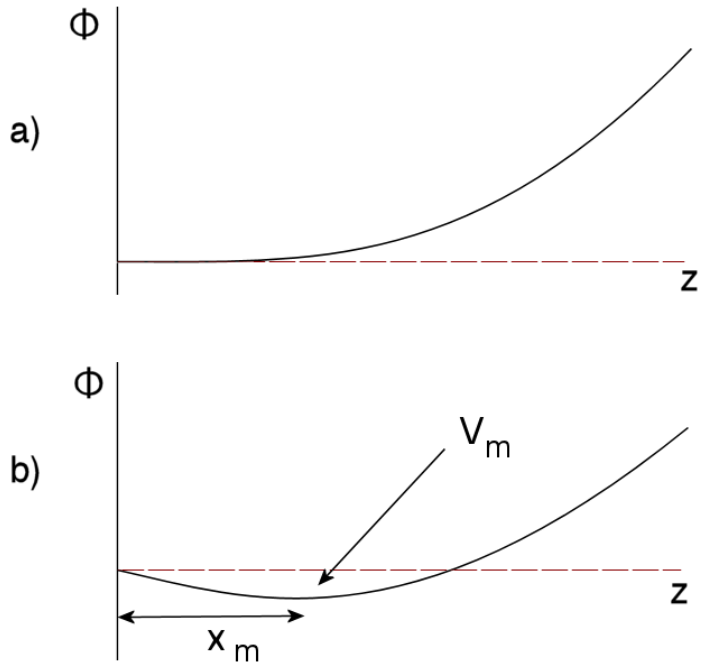

Figure 1: Variation of electrostatic potential near the surface of a cathode under the condition of space-charge-limited emission. *a*) Zero-temperature electrons. *b*) Hot electrons. The quantity V_m is the height of the potential barrier and x_m is the sheath width, the point where $d\phi/dz = 0.0$.

The zero-energy model raises some logical issues:

If all electrons on the surface are identical, what determines whether an individual electron enters the flow?

How can we account for a flux to the surface if the electrons are cold?

For a realistic model, we must consider a thermal distribution of incident electrons. If the thermal flux of current, j_t, exactly equals the current density of Eq. 1, then every electron is extracted and E_z is almost zero at the cathode surface. If we raise the cathode temperature so that $j_t > j_c$, a region of depressed potential is created as in Fig. 1*b*. The potential barrier $-V_m$ allows only a fraction $\sim j_c/j_t$ of the incident electrons to pass. The other electrons reflect back to the cathode. This process is described by the Langmuir theory[5] and by the calculations of this paper.

2 Numerical model

The goal is to find equilibrium solutions, so I applied ray-tracing [6] rather than the particle-in-cell method. For a given run time, ray tracing gives higher statistical accuracy for steady-state particle flows. The idea is to generate a distribution of N_p model electrons near $z = 0.0$ with appropriate values of speed and direction to represent a thermal distribution. If the target thermal flux of current is j_t, then each model particle is assigned a current density $j_0 = j_t/N_p$. The code tracks orbits in the electric field, advancing by time step Δt to determine a sequence of small trajectory segments for each electron. At each time step, the space-charge-density in the mesh cell at the center of the segment is incremented by

$$\Delta\rho = \frac{j_0 \Delta t}{\Delta z}, \tag{2}$$

where Δz is the width of the cell. The electrostatic potential is recalculated with the contribution of beam space charge and the trajectories are retraced in the modified field. The process continues for multiple iterations until the potential converges to a self-consistent solution.

I used a mesh of N_m elements of uniform width $\Delta z = d/N_m$. The potential with space charge was calculated using the back-substitution method[7] with the fixed potential conditions $\phi(0) = 0.0$ and $\phi(D) = V_0$. Trajectories for the non-relativistic electrons were calculated using the two-step method[7], with current-density assignment at the center point of each step. I picked the time step Δt to ensure that the highest energy electrons crossed only half a cell per time step.

Incident electrons at the cathode had an isotropic, Maxwell-Boltzmann distribution. Initial directions were assigned with respect to a polar angle θ (the angle with respect to the z direction) and an azimuthal angle ϕ (the projected direction in the x-y plane). If ξ is a random variable in the range $0.0 \leq \xi \leq 1.0$, then the azimuthal angle is given by

$$\phi = 2\pi\xi. \tag{3}$$

Assignment of the polar angle was weighted so that there were equal numbers of electrons per solid angle in the emission hemisphere:

$$\theta = \sin^{-1}(\xi). \tag{4}$$

Given the angles, the initial direction-vector components were

$$u_x = \cos(\theta)\cos(\phi), \tag{5}$$
$$u_y = \cos(\theta)\sin(\phi), \tag{6}$$
$$u_z = \sin(\theta). \tag{7}$$

To assign kinetic energy, I used a package for cubic spline interpolations of tabular functions. A table consists of ordered values of an independent variable (X) and dependent variable (Y). For a given value of X, the routines return an accurate interpolation of Y. For a Maxwell-Boltzmann distribution with temperature T_e ^{o}K, the probability distribution of kinetic energy U scales as [8]

$$f(U) \sim \sqrt{\frac{U}{kT_e}}\ \exp\left(-\frac{U}{kT_e}\right). \tag{8}$$

I set up a spreadsheet to carry out a numerical integration to create set of 100 values of the normalized function

$$F(U) = \frac{\int_0^U f(U')dU'}{\int_0^{U_{max}} f(U')dU'} \tag{9}$$

I used a high-energy cutoff $U_{max} = 6kT_e$. The values were inserted into a tabular function to perform an inversion, $Y = U$, $X = F(U)$. The procedure to assign kinetic energy was to set the X value equal to a normalized random variable ξ and then to find the return value of U from a table interpolation.

To test the method, the code recorded the initial electron parameters in the standard format of the Field Precision **GenDist** program for distribution analyses. Figure 2 shows results for 10,000 model electrons with $kT_e = 1.0$ eV. The probability distribution in θ is proportional to $\sin(\theta)$ as expected for a uniform distribution in solid angle. The distribution in kinetic energy

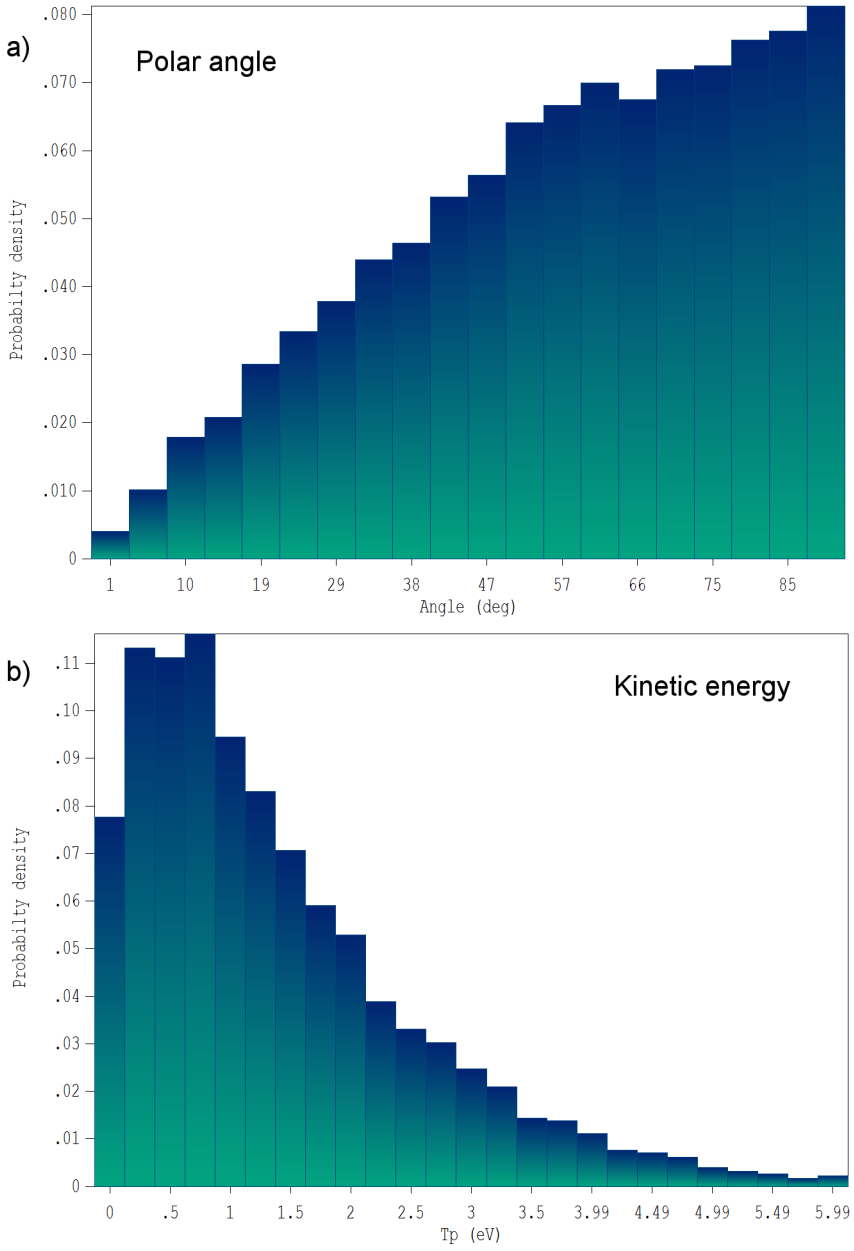

Figure 2: Initial distribution of particles at the cathode. *a*) Angle with respect to the surface normal vector. *b*) Kinetic energy for $kT = 1.0$ eV.

follows Eq. 8. The average kinetic energy of the electron distribution is 1.455 eV. The small difference from the theoretical value of 1.500 is a consequence of truncation of the distribution at high energy.

3 Results

Calculations were performed for the specific parameters $d = 0.01$ m and $V_0 = 100.0$ V. Nonetheless, the results may be applied to any electron or ion extraction gap by identifying scaling parameters:

> kT_e/eV_0, the ratio of the injected thermal energy to the energy gained by acceleration.
>
> j_t/j_c, the ratio of the injected thermal charge flux to the Child current density at zero temperature. For the baseline parameters, Eq. 1 gives a zero-temperature current density $j_c = 23.3$ A/m^2.

We can also define scaling laws for the Langmuir parameters (defined in Fig. 1). The height of the potential barrier should be proportional to the incident electron kinetic energy,

$$eV_m \sim kT_e \tag{10}$$

The following scaling law is useful for the sheath width:

$$\frac{x_m}{D} \sim \frac{kT_e}{eV_0}. \tag{11}$$

Both quantities should increase with (j_t/j_s).

A goal of the calculations was to find the effect of electron temperature on the space-charge-limited current density. I investigated a range of relative electron temperatures $0.001 \leq kT_e/eV_0 \leq 0.100$. An accurate resolution of the sheath was necessary for numerical stability, $\Delta z \ll x_m$. At the lowest values of temperature, I used a mesh with small elements ($N_m = 2500$). For good statistics, the runs included 5000 model electrons. To avoid the cycle-to-cycle oscillations that sometimes occur in ray-tracing solutions, I adjusted the mesh space-charge values gradually according to

$$\rho = \alpha\rho_{new} + (1 - \alpha)\rho_{old}. \tag{12}$$

In Eq. 12, ρ_{new} is the space-charge density of particles in the present cycle and ρ_{old} is an average over previous cycles. Good convergence was obtained with $\alpha = 0.20$ and 100 cycles. The code kept a convergence record, recording the quantity $\Delta\rho_{RMS}/\rho_{avg}$ averaged over all cells. The residual was quite small

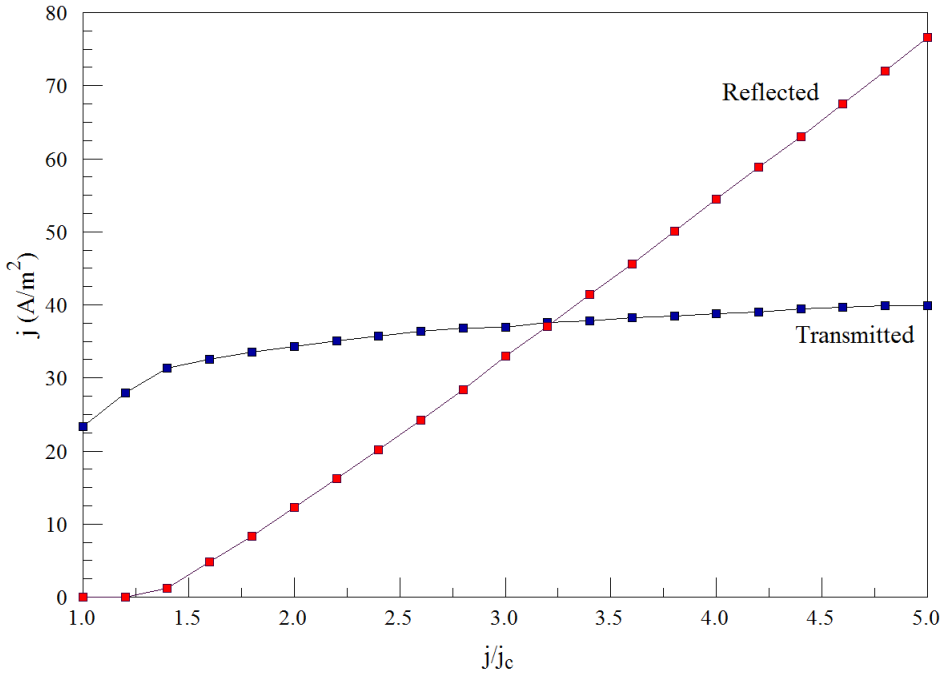

Figure 3: Transmitted and reflected current as a function of (j_t/j_c) for $kT_e/eV_0 = 0.05$.

($\sim 10^{-8}$) for $j_t/j_c = 1.0$, but was typically 10^{-3} when there were reflected electrons. With tiny changes in the sheath potential, a few of the model electrons with initial energy close to eV_m oscillated between transmission and reflection on different cycles. The effect was small, and the convergence level corresponded to good overall accuracy.

For each value of (kT_e/eV_0), the code carried out a series of runs over the range $1.0 \leq j_t/j_c \leq 5.0$. The upper limit reflects the fact that it would be impractical to run a cathode at very high temperates to create a thermal current flux much higher than the extractable current density. Figure 3 shows raw data for $(kT_e/eV_0) = 0.05$. At $(j_t/j_c) = 1.0$, all electrons were transmitted. Reflected electrons occurred when the thermal flux exceeded the temperature-adjusted space-charge limit. At high values of (j_t/j_c), the reflected current increased without limit while the transmitted current density approached a constant value. For lower values of (kT_e/eV_0), saturation occurred at lower values of (j_t/j_c).

Figure 4 gives a normalized plot of saturated transmitted current density for the full set of runs. Note that the values converged to 1.00 when $(kT_e/eV_0) \ll 1.0$, a good check of the numerical accuracy of the code. The dashed line is a fit to the data:

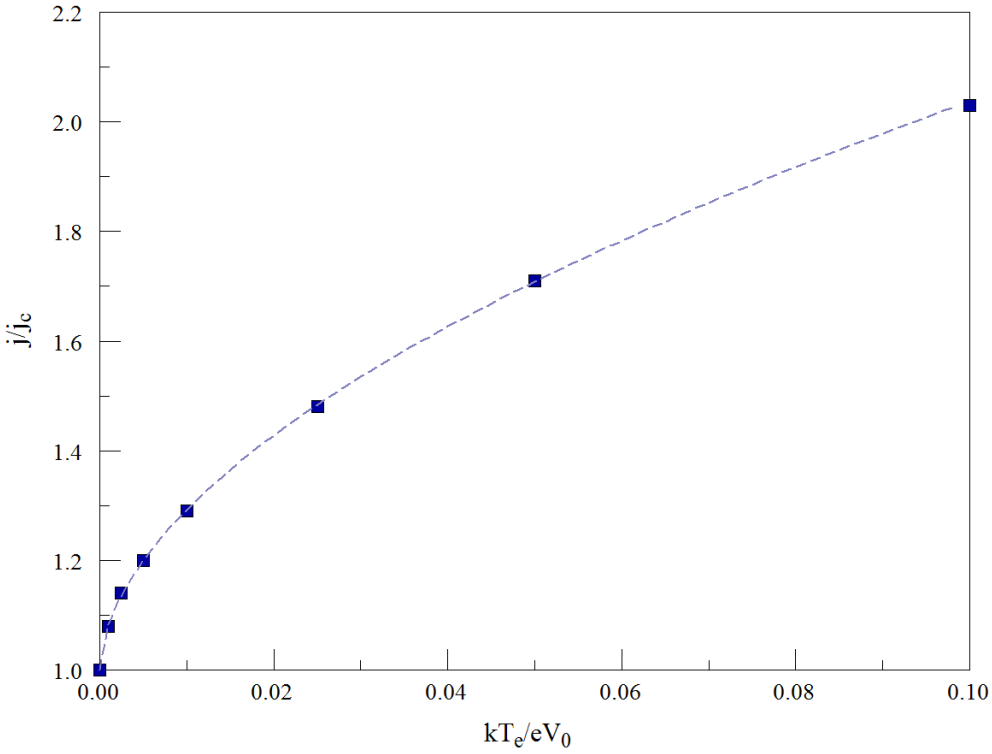

Figure 4: Normalized transmitted current density as a function of normalized temperature for $(j_t/j_c) \gg 1.0$. Dashed line shows the function of Eq. 13. The point at (0.0, 1.0) was added.

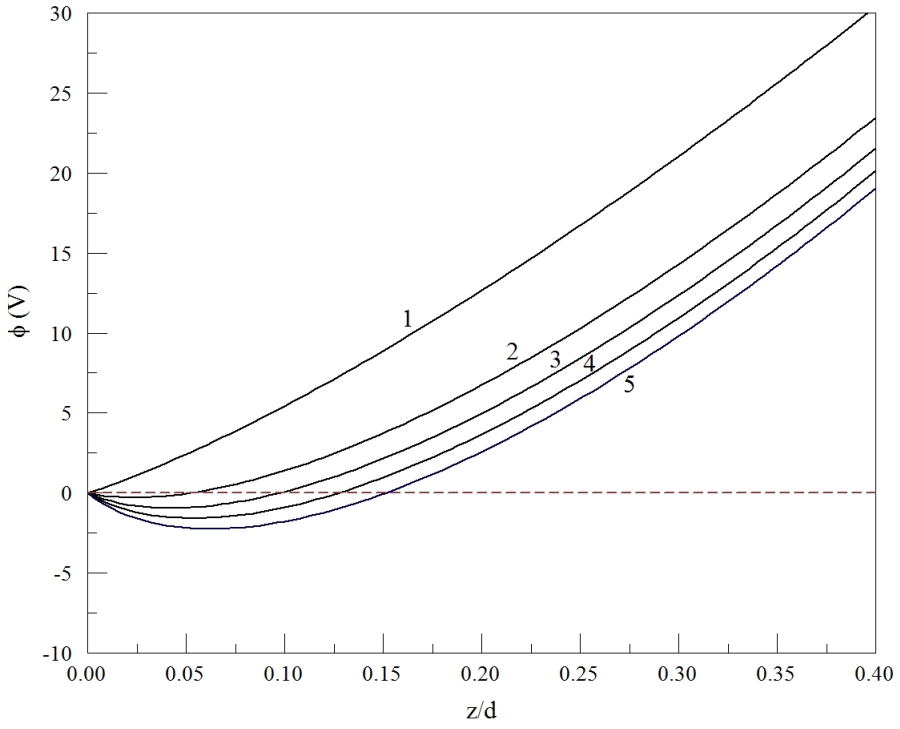

Figure 5: Sheath potential near the cathode for $(kT_e/eV_0 = 0.05)$ and $(j_t/j_c) = 1.0, 2.0, 3.0, 4.0$ and 5.0.

$$j_s/j_c \cong 1.0 + 3.68 \left(\frac{kT_e}{eV_0}\right)^{0.55} . \tag{13}$$

Figure 5 shows how the potential barrier increases with the available thermal flux. The code results can be used to create plots of the Langmuir sheath properties, V_m and x_m. From plots like Fig. 5, it is possible to estimate the depth and position of the point where $d\phi/dz = 0.0$. Results for the full set of solutions are displayed in Fig. 6 using the scaling of Eqs. 10 and 11. In both plots, the abscissa is the ratio of incident thermal charge flux to the zero-temperature Child limit. The scaling relations proved useful, compressing data corresponding to a factor of 100 variation in electron temperature to a limited plot range. As expected, V_m and x_m increased with (j_t/j_c).

The final issue was to investigate whether sheath processes contributed to changes in the transverse temperature of the transmitted beam. My original hypothesis was that velocity selection at the sheath could contribute to beam cooling. At high values of (j_t/j_c), only electrons with the highest longitudinal energy could cross the potential barrier to contribute to the transmitted beam. Perhaps these electrons would, on average, have lower transverse energy. Under this theory, the angular divergence of the transmitted beam

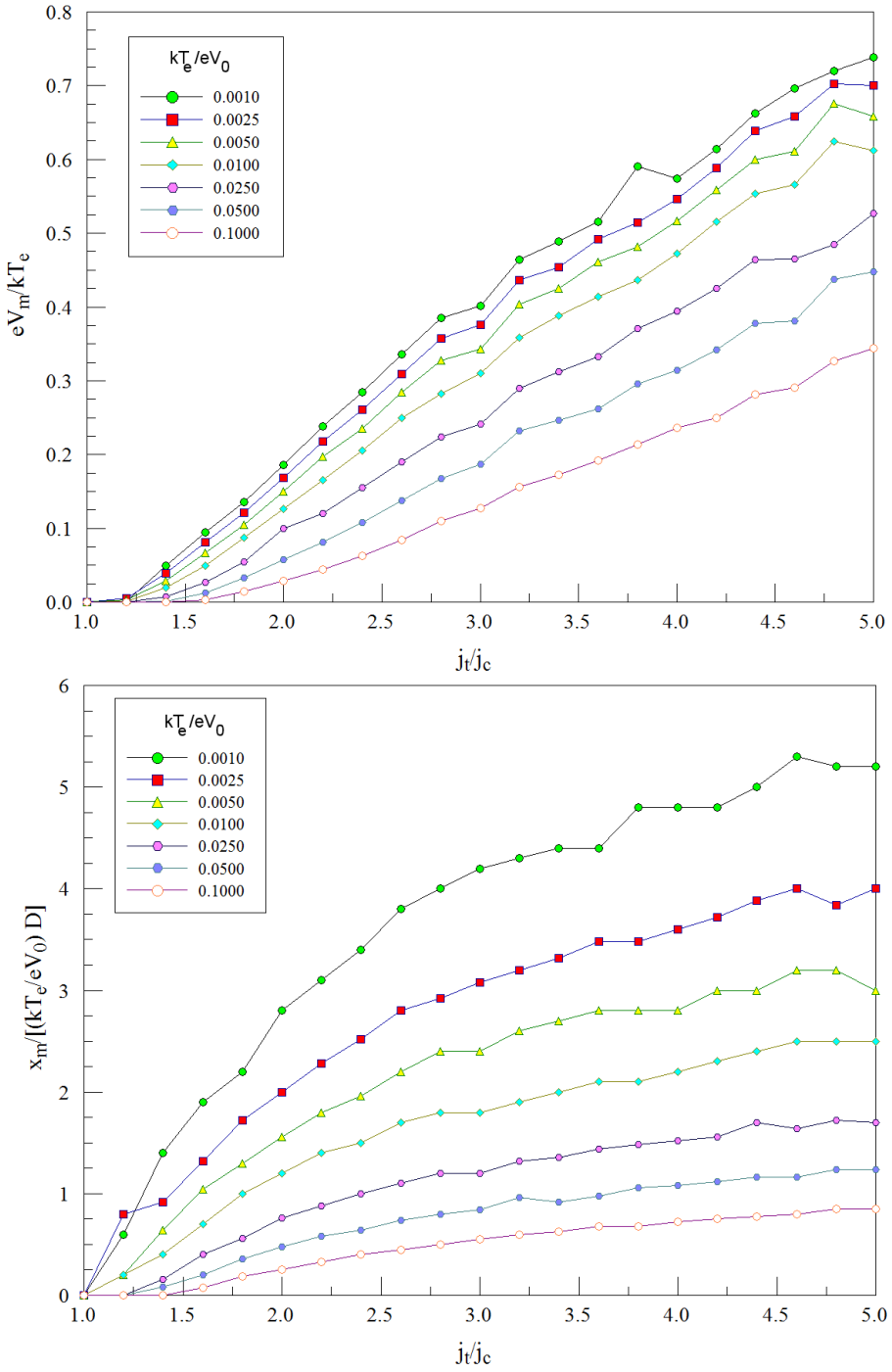

Figure 6: Calculated sheath properties. *a*) Normalized potential barrier height as a function of (j_t/j_c). b) Normalized sheath width as as a function of (j_t/j_c).

would decrease with increasing (j_t/j_c). Accordingly, I included routines in the code to collect only transmitted electrons in the converged solution and to analyze their root-mean-squared divergence angle. The results are plotted in Fig. 7. The divergence increased with kT_e as expected, but there was no dependence on (j_t/jc) whatever. In retrospect, this was precisely the behavior one would expect from theory. Because there are no forces in the x and y directions, the transverse temperature of the electrons was invariant. In the presence of a potential barrier, the density of particles in a Maxwell-Boltzmann distribution changes, but the temperature does not. In other words, the velocity distribution of electrons $f(v_z)$ is the same at all positions $z \leq x_m$. Therefore, the ratio of transverse to longitudinal spread does not depend on the height or position of the sheath. Note that the slight decrease in angle at the highest temperature is the result of truncating the Maxwell-Boltzmann distribution.

In summary, there are three results of this work:

Figure 4 and Eq. 13 may be applied to estimate the magnitude of space-charge-limited current density in an acceleration gap with a relatively high electron temperature.

Figure 6 is useful to estimate the height and width of the extraction sheath for thermal electrons.

There is no velocity-selection process in the thermal sheath of a space-charge-limited extraction gap. Therefore, the cathode temperature can be used to estimate the divergence angle of extracted beams in codes like **Trak** and **OmniTrak**.

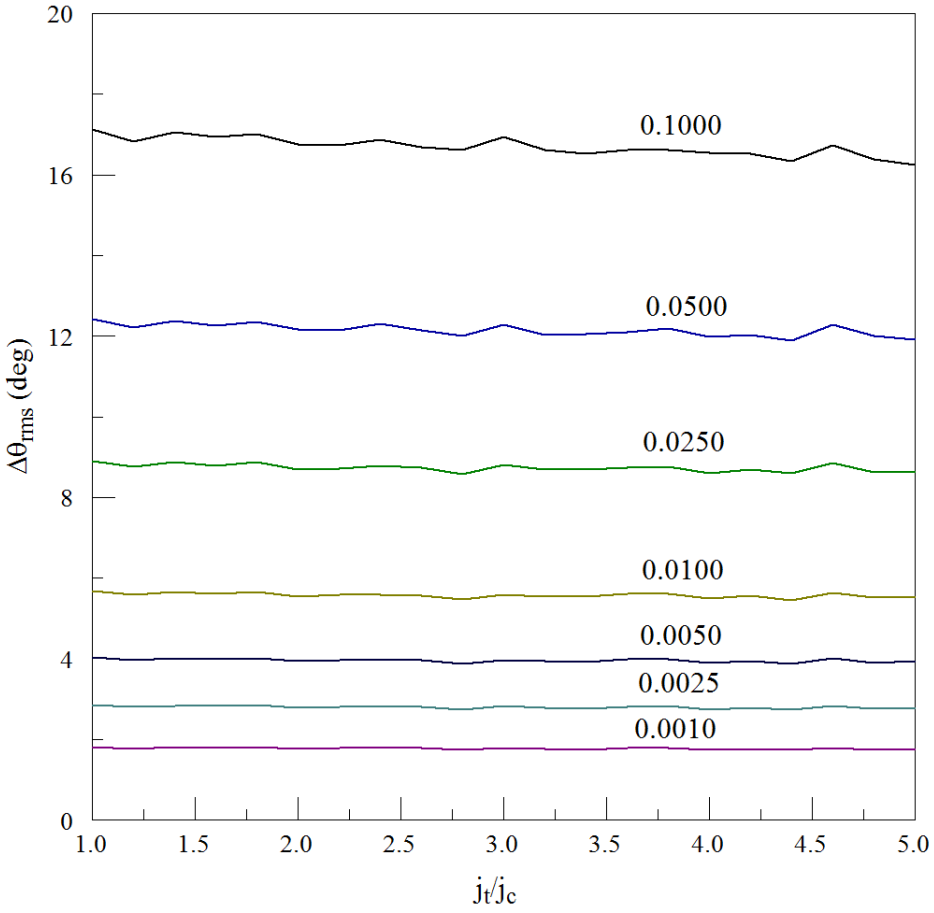

Figure 7: Root-mean-squared divergence angle of the transmitted beam as a function of (j_t/j_c) and (kT_e/eV_0).

References

[1] C.D. Child, Phys. Rev. **32**, 492 (1911).

[2] W. Schottky, Phys. Zeits **15**, 526 and 624 (1914).

[3] T.C. Fry, Phys. Rev. **17**, 441 (1921).

[4] T.C. Fry, Phys. Rev. **22**, 445 (1923).

[5] I. Langmuir, Phys. Rev. **21**, 419 (1923)

[6] See, for instance, S. Humphries, **Charged Particle Beams** (Wiley, New York, 1990), 279.

[7] See, for instance, S. Humphries, **Field Solutions on Computers** (CRC Press, Boca Raton, 1997), 71 and 75.

[8] D.J. Rose and M. Clark, **Plasmas and Controlled Fusion** (MIT Press, Cambridge, 1961), 62.